Table 1 Integrated flux densities for the two components of L1551 IRS5

Wavelength	A (North)	B (South)	Interferometer	Reference
18 cm	0.70 ± 0.20	0.60 ± 0.20	MERLIN	*
3.6 cm	0.78 ± 0.02	0.70 ± 0.02	VLA	This work
2.0 cm	1.2 ± 0.1	0.9 ± 0.1	VLA	20
1.3 cm	2.0 ± 0.2	1.5 ± 0.2	VLA	†
7.0 mm	7.4 ± 0.5	4.8 ± 0.5	VLA	This work
2.7 mm	45 ± 6	23 ± 6	BIMA	26

Flux densities are in mJy.
* S. Curiel *et al.*, manuscript in preparation.
† D. W. Koerner and A. I. Sargent, manuscript in preparation.

still accrete from the circumbinary disk, via gas streams that move across the tidal gap. Under these circumstances, accretion will occur preferentially into the lower mass component of the system, driving the mass ratio towards unity, as observed in L1551 IRS5.

In the case of the visible T Tauri stars, which are sources more evolved than L1551 IRS5, there is evidence[7,8] that the stars constituting a close binary (that is, a pair with separation of less than 100 AU) have less millimetre emission than single stars or wide binaries. This result has been taken to indicate that the gravitational interactions between the members of the binary result in less massive disks. In the case of extremely young stars like L1551 IRS5, there are no data available yet to search for similar tendencies. □

Received 19 March; accepted 26 June 1998.

1. Beckwith, S. V. W. & Sargent, A. I. Circumstellar disks and the search for neighbouring planetary systems. *Nature* **383,** 139–144 (1996).
2. Reipurth, B. & Zinnecker, H. Visual binaries among pre-main sequence stars. *Astron. Astrophys.* **278,** 81–108 (1993).
3. Leinert, C. *et al.* A systematic approach for young binaries in Taurus. *Astron. Astrophys.* **278,** 129–149 (1993).
4. Simon, M. *et al.* A lunar occultation and direct imaging survey of multiplicity in the Ophiuchus and Taurus star-forming regions. *Astrophys. J.* **443,** 625–637 (1995).
5. Ghez, A. M., McCarthy, D. W., Patience, J. L. & Beck, T. L. The multiplicity of pre-main-sequence stars in southern star-forming regions. *Astrophys. J.* **481,** 378–385 (1997).
6. Artymowicz, P. & Lubow, S. H. Dynamics of binary-disk interaction. 1: Resonances and disk gap sizes. *Astrophys. J.* **421,** 651–667 (1994).
7. Jensen, E. L. N., Mathieu, R. D. & Fuller, G. A. The connection between submillimeter continuum flux and binary separation in young binaries: Evidence of interaction between stars and disks. *Astrophys. J.* **458,** 312–326 (1996).
8. Osterloh, M. & Beckwith, S. V. W. Millimeter-wave continuum measurements of young stars. *Astrophys. J.* **439,** 288–302 (1995).
9. Lay, O. P., Carlstrom, J. E., Hills, R. E. & Phillips, T. G. Protostellar accretion disks resolved with the JCMT-CSO interferometer. *Astrophys. J.* **434,** L75–L78 (1994).
10. Mundy, L. G. *et al.* Imaging the HL Tauri disk at lambda = 2.7 millimeters with the BIMA array. *Astrophys. J.* **464,** L169–L173 (1996).
11. Wilner, D. J., Ho, P. T. P. & Rodríguez, L. F. Subarcsecond VLA observations of HL Tauri: Imaging the circumstellar disk. *Astrophys. J.* **470,** L117–L121 (1996).
12. Mannings, V., Koerner, D. W. & Sargent, A. I. A rotating disk of gas and dust around a young counterpart to β Pictoris. *Nature* **388,** 555–557 (1997).
13. Strom, K. M., Strom, S. E. & Vrba, F. J. Infrared surveys of dark-cloud complexes. IV. The Lynds 1517 and Lynds 1551 clouds. *Astron. J.* **81,** 320–322 (1976).
14. Butner, H. M., Evans, N. J., Lester, D. F., Levreault, R. M. & Strom, S. E. Testing models of low-mass star formation—High-resolution far-infrared observations of L1551 IRS 5. *Astrophys. J.* **376,** 635–653 (1991).
15. Torrelles, J. M. *et al.* Are interstellar toroids the focusing agent of the bipolar molecular outflows? *Astrophys. J.* **274,** 214–230 (1983).
16. Saito, M., Kawabe, R., Kitamura, Y. & Sunada, K. Imaging of an infalling disklike envelope around L1551 IRS 5. *Astrophys. J.* **473,** 464–469 (1996).
17. Keene, J. & Masson, C. R. Detection of A 45 AU radius source around L1551-IRS5—A possible accretion disk. *Astrophys. J.* **355,** 635–644 (1990).
18. Lay, O. P., Carlstrom, J. E., Hills, R. E. & Phillips, T. G. Protostellar accretion disks resolved with the JCMT-CSO interferometer. *Astrophys. J.* **434,** L75–L78 (1994).
19. Bieging, J. H. & Cohen, M. Multifrequency radio images of L1551 IRS 5. *Astrophys. J.* **289,** L5–L8 (1985).
20. Rodríguez, L. F., Cantó, J., Torrelles, J. M. & Ho, P. T. P. The double radio source associated with L1551 IRS 5—Binary system or ionized circumstellar torus? *Astrophys. J.* **301,** L25–L28 (1986).
21. Snell, R. L., Loren, R. B. & Plambeck, R. L. Observations of CO in L1551—Evidence for stellar wind driven shocks. *Astrophys. J.* **239,** L17–L22 (1980).
22. Rodríguez, L. F. in *Herbig-Haro Flows and the Birth of Low Mass Stars* (eds Reipurth, B. & Bertout, C.) 83–92 (Proc. IAU Symp. 182, Kluwer, Dordrecht, 1997).
23. Moriarty-Schieven, G. H. & Wannier, P. G. A second outflow from L1551/IRS 5? *Astrophys. J.* **373,** L23–L26 (1991).
24. Pound, M. W. & Bally, J. Two new molecular outflows in L1551? *Astrophys. J.* **383,** 705–713 (1991).
25. Fridlund, C. V. M., Huldtgren, M. & Liseau, R. in *Herbig-Haro Flows and the Birth of Low Mass Stars* (eds Reipurth, B. & Bertout, C.) 19–28 (Proc. IAU Symp. 182, Kluwer, Dordrecht, 1997).
26. Looney, L. W., Mundy, L. G. & Welch, W. J. High-resolution lambda = 2.7 millimeter observations of L1551 IRS 5. *Astrophys. J.* **484,** L157–L160 (1997).
27. Boss, A. P. Evolution of the Solar Nebula. III. Protoplanetary disks undergoing mass accretion. *Astrophys. J.* **469,** 906–920 (1996).
28. D'Alessio, P., Calvet, N. & Hartmann, L. The structure and emission of accretion disks irradiated by infalling envelopes. *Astrophys. J.* **474,** 397–406 (1997).
29. Mathieu, R. D. Pre-main-sequence binary stars. *Annu. Rev. Astron. Astrophys.* **32,** 465–530 (1994).
30. Duquennoy, A. & Mayor, M. Multiplicity among solar-type stars in the solar neighbourhood. II—Distribution of the orbital elements in an unbiased sample. *Astron. Astrophys.* **248,** 485–524 (1991).
31. Artymowicz, P. & Lubow, S. H. Mass flow through gaps in circumbinary disks. *Astrophys. J.* **467,** L77–L80 (1996).

Acknowledgements. We appreciate the open policy of the National Radio Astronomy Observatory, which is a facility of the US National Science Foundation operated under cooperative agreement by Associated Universities, Inc. In particular, we thank the NRAO personnel involved in the 7-mm upgrade. The 7-mm receivers used for these observations were built with the support of CONACyT, México. We thank A. Poveda for his comments on binary stars.

Correspondence should be addressed to L.F.R. (e-mail: luisfr@astrosmo.unam.mx).

Continuous excitation of planetary free oscillations by atmospheric disturbances

Naoki Kobayashi* & Kiwamu Nishida*†

** Earth and Planetary Sciences, Tokyo Institute of Technology, Meguro, Tokyo 152, Japan*

Seismology provides a powerful tool for probing planetary interiors[1,2], but it has been considered inapplicable to tectonically inactive planets where earthquakes are absent. Here, however, we show that the atmospheres of solid planets are capable of exerting dynamic pressure on their surfaces, thereby exciting free oscillations with amplitudes large enough to be detected by modern broad-band seismographs. Order-of-magnitude estimates of these forces give similar amplitudes of a few nanogals for the Earth, Venus and Mars despite widely varying atmospheric and ambient conditions. The amplitudes are also predicted to have a weak frequency dependence. Our analysis of seismograms, recorded continuously from 1992 to 1993 at 13 globally distributed stations, shows strong evidence for continuously excited fundamental-mode free oscillations on the Earth. This result, together with other recent studies[3–5], is consistent with our estimate of atmospheric forcing and we therefore propose that it may be possible to detect atmospheric excitation of free oscillations on Venus and Mars as well.

The Sun pulsates owing to acoustic waves generated by intensive turbulent gaseous motion on the top of the convective layer[6]. Similar processes should occur on solid planets having atmospheres, and should excite seismic waves that propagate throughout the solid interior, thereby inducing free oscillations. Such planetary atmospheric disturbances should occur even on tectonically inactive solid planets such as Mars and Venus.

We now estimate the order of magnitude of the seismic free oscillations excited by atmospheric disturbances. Some atmospheric gases such as water vapour and carbon dioxide cause a so-called greenhouse effect[7]. Atmospheres are relatively transparent to visible light but have strong absorption at infrared wavelengths[8]. Visible light absorbed at and near the surface is converted and re-radiated at infrared wavelengths. The infrared rays are absorbed into the atmosphere and warm the air near the surface. The resultant buoyant force induces atmospheric convective motions. In a steady state, the heat flux transported by the atmosphere must be balanced by the net solar influx:

$$\frac{v^2}{H} = g\alpha\Delta T \tag{1}$$

$$S(1-A)/4 = \rho_{at} C_p \Delta T v \tag{2}$$

Symbols used are defined in Table 1. From the above equations, the amplitude of the velocity fluctuation is:

$$v = (g\alpha S(1-A)H/4\rho_{at}C_p)^{1/3} \tag{3}$$

† Present address: Earthquake Research Institute, University of Tokyo, Tokyo, Japan.

The associated dynamic pressure fluctuation is scaled by $p_0 = \rho_{at} v^2$, and pressure disturbances with timescale $1/f$ (where f is frequency) are:

$$\delta p = p_0 \frac{f_0}{f} \quad (4)$$

where $1/f_0 = H/v$ is the timescale of convective motion. This frequency dependence is obtained from dimensional considerations. To construct the dimension of pressure in terms of S, H and time $1/f$, we require S/Hf, to which the right-hand side of equation (4) is proportional. Although equation (4) was constructed by dimensional analysis, it is consistent with observations of atmospheric pressure. Here we consider only temporal variations of convective cellular motions whose scale is about H. Smaller-scale turbulence may be important for generation of acoustic waves in the atmosphere, but is less effective in generating elastic waves in the solid portion of the planet.

Fluctuations of pressure loading on the surface of the solid portion will preferentially excite fundamental spheroidal modes, because their elastic energy is confined to shallower depths than overtone modes. Here we use a simplified form of the comprehensive theory of excitation of free oscillations[9] to assess the excited amplitudes of fundamental spheroidal modes. We consider a steady state in which a balance is achieved between energy input from atmosphere to a mode (energy input rate G) and dissipation of its elastic energy E (the dissipation rate ΓE) in the same manner as is done in helioseismology[10]:

$$G = \Gamma E = \frac{\omega}{Q} E \quad (5)$$

Here $E \approx \omega^2 M_e d^2/2$, where d is displacement, ω is angular frequency and M_e is effective elastic mass (solid density × surface area × penetration depth of the elastic energy). The input power is $G = \omega dF$, where the force exerted on a mode is $F = 4\pi R^2 \delta p/L$. The cut-off angular order is $L = 2\pi R/H$. We assume that the horizontal correlation length of the random atmospheric disturbance is approximately equal to H, and the spatial power of the disturbance is equipartitioned into L^2 modes. From the above equations, we obtain the amplitude of the excited acceleration:

$$a = \omega^2 d = \frac{QHp_0 f_0}{\pi R \rho_{sol} \lambda f} = \frac{QHp_0 f_0}{\pi R \rho_{sol} c} \quad (6)$$

where we use the horizontal wavelength $\lambda = c/f$ as the penetration depth. The frequency dependence of this amplitude is weak, as the quality factor Q and the surface-wave phase velocity c are not strongly dependent on frequency in the millihertz band. Using typical values for various parameters, we obtain amplitudes of the order of nanogals (10^{-11} m s^{-2}) for the Earth, Venus and Mars (Table 1) in spite of greatly differing solar energy input rates, planetary masses and atmospheric densities. Such amplitudes are detectable by standard broad-band seismographs[11,12].

We have analysed continuous records from 13 stations of the Incorporated Research Institutions for Seismology (IRIS) network[13] for 1992–93 to search for continuously excited free oscillations of the Earth. The instruments are STS-1[11] very broad-band seismometers. We selected the 13 stations which have the lowest ground noise level (slightly less than 10^{-18} m^2 s^{-4} Hz^{-1} in the millihertz band) in the IRIS station catalogue. For each station, we produced a spectrogram (a contour plot of power spectral density in the frequency–time plane) after removing glitches, nonlinear responses due to large earthquakes, and tidal components: we divided the data into segments of about a half day long with overlaps of about a quarter of a day. We then calculated power spectral densities for each segment using Weltch tapering, and lined up the spectrograms with respect to time. These spectrograms show intervals with large oscillations excited by earthquakes of various magnitudes.

To exclude signals due to earthquakes with seismic moment $M_0 > 10^{17}$ N m, we calculated the power $A_5(t_0)$ of segments in the band from 2.5 to 7.5 mHz (based on the Harvard Centroid-Moment Tensor (CMT) catalogue[14]) and discarded segments from the origin time until the time when $A_5(t_0)\exp[-f(t-t_0)/Q]$ ($f = 5$ mHz and $Q = 200$) becomes less than 5.0×10^{-22} m^2 s^{-4} (about a tenth of the noise level). We also discarded segments in which the power $A_{10}(t)$ in the band from 7.5 to 12.5 mHz is larger than 5.0×10^{-21} m^2 s^{-4} to exclude the effects of local smaller earthquakes and other transient phenomena. Further details will be presented elsewhere (K.N. and N.K., manuscript in preparation). The criteria for identifying continuous signals that we interpret as atmospherically excited free oscillations are as follows: (1) fundamental spheroidal modes are selectively excited with nanogal acceleration in a broad frequency range, (2) weak frequency dependence of the amplitudes.

Figure 1a shows selected data at SUR, which is one of the quietest stations. Weak but definite vertical stripes at the frequencies of fundamental spheroidal modes are identified. An ensemble average of the power spectral density is shown in Fig. 1b. From 3 to 7 mHz, distinct peaks are observed at the frequencies of the fundamental spheroidal modes. The power spectral densities are about 1×10^{-18} m^2 s^{-4} Hz^{-1} and do not show marked dependence on the frequency. To estimate the acceleration, we multiplied these peak values by the full width at half the peak value and took the square root. The obtained values are slightly less than 1×10^{-11} m s^{-2}, that is, 1 nGal. This is consistent with our order-of-magnitude estimate (above) for the amplitude of free oscillations due to continuous atmospheric excitation. We obtained similar results from other stations (Fig. 2).

Continuously excited signals with frequency-independent amplitudes at the nanogal level have also been observed in other studies[3–5]. These results, taken together, suggest the existence of continuously excited free oscillations in a broad frequency range from 0.3 to 7 mHz. Nawa *et al.*[3] reported seasonal variations in amplitude (higher amplitudes in the period from May to September), but we have not yet confirmed seasonal variations in our data. It is necessary to use a longer time series to clearly verify the existence of seasonal variations, because variations of only ~10% are expected.

Table 1 Physical parameters and excited amplitudes

	S (W m^{-2})	A	ρ_{at}* (kg m^{-3})	T (K)	R (10^6 m)	g (m s^{-2})	H (10^4 m)	C_p (J K^{-1} kg^{-1})	v (m s^{-1})	p_0 (Pa)	τ_0 (10^3 s)	a† (nGal)
Venus	2,620	0.78	65.3	750	6.03	8.9	1.58	657	0.9	48	18	2.2
Earth	1,370	0.30	1.16	290	6.38	9.8	0.87	1,030	3.8	17	2.2	3.4‡
Mars	590	0.16	1.33×10^{-2}	240	3.40	3.7	1.21	657	13	2.6	0.88	3.3

Here S is solar energy flux, A albedo, ρ_{at} density of atmosphere at surface, T surface temperature, R radius of planet, g surface gravity, H pressure scale height, C_p specific heat at constant pressure, v and p_0 are scales of velocity and pressure fluctuations, respectively, and $\tau_0 = 1/f_0$ is timescale of convective motions in the atmosphere.
* We treat atmospheres as diatomic ideal gases. Molecular weights are 44, 28 and 44 for Venus, Earth and Mars, respectively.
† We used solid density $\rho_{sol} = 4 \times 10^3$ (kg m^{-3}), surface wave velocity $c = 5 \times 10^3$ (m s^{-1}) and quality factor $Q = 200$ to evaluate the resultant amplitudes. These values are typical for fundamental spheroidal modes in the millihertz band. We also used these values for Venus and Mars.
‡ On the Earth, energy is carried by not only sensible heat but also by latent heat of water vapour. If we take the latent heat in our estimate, the excitation amplitude has the somewhat smaller value of ~0.8 nGal.

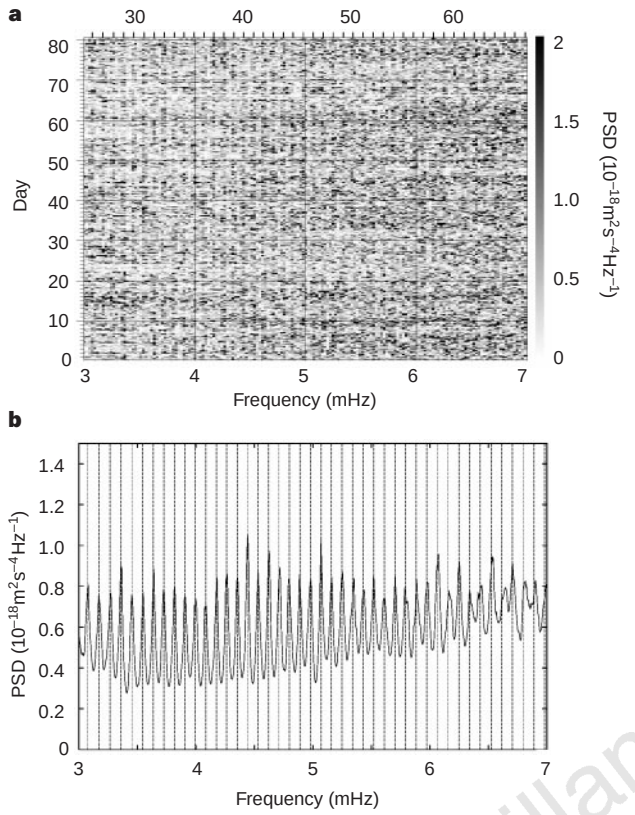

Figure 1 Earth's free oscillations on the quietest days. **a**, A selected spectrogram obtained from the IRIS data at SUR (Southerland, Republic of South Africa) in 1992–93. Grey-scale at right shows spectral power density. Dark vertical stripes can be seen at the frequencies of fundamental spheroidal modes of the spherically symmetric Earth model (PREM)[2]. The level of the stripes is $\sim 1 \times 10^{-18}$ m^2 s^{-4} Hz^{-1}. Tick marks on the upper *x*-axis show the frequencies of spheroidal fundamental modes (from ${}_0S_{22}$ to ${}_0S_{65}$). We cannot see any free oscillation signals outside this frequency range. **b**, Ensemble average of power spectral densities (PSD) of **a**. The distinct peaks correspond to the eigenfrequencies of fundamental spheroidal modes. The vertical lines show locations of the eigenfrequencies of PREM[2] from ${}_0S_{22}$ to ${}_0S_{65}$. Each peak just overlaps the vertical line. We can roughly estimate the acceleration amplitudes by multiplying peak values by full width at half the peak value and taking the square root. The amplitudes of slightly less than 1 nGal and the weak frequency-dependence are consistent with our estimates.

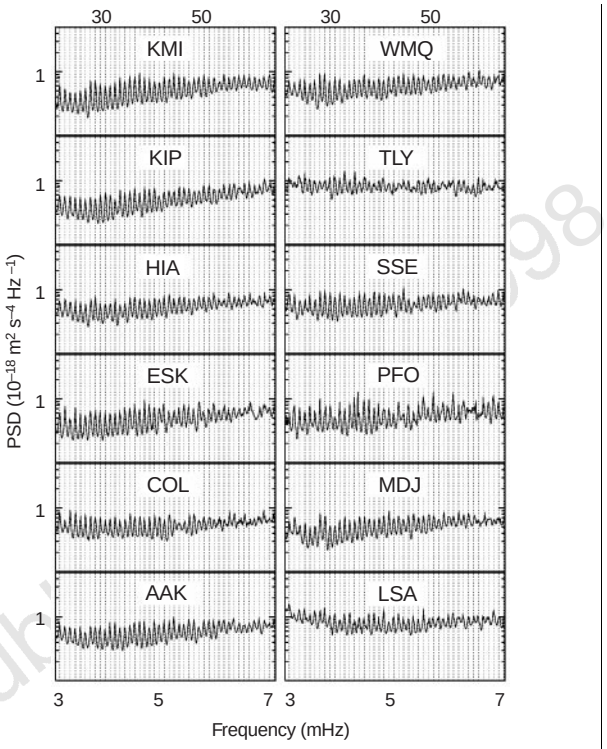

Figure 2 Continuously excited free oscillations were observed globally. Diagrams were produced in the same way as Fig. 1b for 12 different stations: KMI (Kunming, China), KIP (Kipapa, Hawaii, USA), HIA (Hailar, China), EK (Eskdalemuir, UK), COL (College, Alaska, USA), AAK (Ala Archa, Kyrgyzstan), WMQ (Urumqi, China), LY (Talaya, Russia), E (Sheshan, China), PFO (Pinyon Flat, California, USA), MDJ (Mutanjiang, China), LSA (Lhasa, China). The results are similar to those for SUR. The frequencies of the peaks are essentially equal in all of these figures, and they agree with the eigenfrequencies of fundamental spheroidal modes of PREM[2]. This is strong evidence that the observed peaks are truly the Earth's free oscillations because they are observed globally at the same level.

Although we attempted to exclude the influence of earthquakes in our analysis, we consider further whether the observed continuously excited oscillations might have been driven by earthquakes. Small earthquakes (with seismic moment $M_0 < 10^{17}$ N m and not listed in the CMT catalogue) might induce incessant low-amplitude free oscillations. To evaluate the amplitudes of steady-state free oscillations excited by small earthquakes, we calculated the mean seismic moment release rate $\langle \dot{M}_0 \rangle$ using the well known (Gutenberg–Richter) magnitude–frequency relation[15] in the seismic moment range from 0 to 10^{17} N m, and obtained $\langle \dot{M}_0 \rangle = 2 \times 10^{12}$ N m s^{-1}. Then the amplitudes are written as;

$$a = \frac{2\langle \dot{M}_0 \rangle}{\Gamma \lambda M_e} = \frac{\langle \dot{M}_0 \rangle Qf}{(2\pi cR)^2 \rho_{sol}}, \qquad (7)$$

where a is roughly proportional to f and $a \approx 1 \times 10^{-3}$ nGal at 3 mHz. Thus we conclude that the observed continuously excited free oscillations were not excited by earthquakes. Another candidate for the origin of the observed signals is slow earthquakes, which could selectively excite low-frequency modes[16]. To examine this possibility, we carefully searched for abrupt and coherent excitation of low-frequency modes in our spectrograms, but no instance of such signals was found. We also considered the possibility of oceanic excitation but, for the following reasons, this mechanism is less effective than atmospheric excitation. First, convective motions in the ocean are weak mainly because the input energy (mean heat flow from the ocean bottom is $\sim 7.8 \times 10^{-2}$ W m^{-2}; ref. 17) is lower than the input solar radiation to the atmosphere. Second, microseisms[15] (seismic waves excited by ocean waves induced by winds) have their maximum power near 100 mHz, far from the free-oscillation band.

We conclude that the Earth's atmosphere can continuously excite detectable free oscillations. The amplitudes and frequency dependence of the observed signals are consistent with our theory. Mars and Venus should also have observable continuously excited fundamental spheroidal mode free oscillations excited by their atmospheres; it should be possible to use such signals to probe the internal structure of these planets, at least the upper-mantle structure. We consider that seismological observations by broad-band seismometers on Mars and Venus are likely to be a promising method of probing their interiors. □

Received 14 November 1997; accepted 22 June 1998.

1. Gilbert, F. & Dziewonski, A. M. An application of normal mode theory to the retrieval of structural parameters and source mechanisms from seismic spectra. *Phil. Trans. R. Soc. Lond. A* **278,** 187–269 (1975).
2. Dziewonski, A. M. & Anderson, D. L. Preliminary reference Earth model. *Phys. Earth Planet. Inter.* **25,** 297–356 (1981).
3. Nawa, K. *et al.* Incessant excitation of the Earth's free oscillations. *Earth Planets Space* **50,** 3–8 (1998).
4. Suda, N., Nawa, K. & Fukao, Y. Earth's background free oscillations. *Science* **279,** 2089–2091 (1998).

5. Tanimoto, T., Um, J., Nishida, K. & Kobayashi, N. Earth's continuous oscillations observed on seismically quiet days. *Geophys. Res. Lett.* **25,** 1553–1556 (1998).
6. Goldreich, P. & Kumar, P. The interaction of acoustic radiation with turbulence. *Astrophys. J.* **326,** 462–478 (1988).
7. Sagan, C. Structure of the lower atmosphere of Venus. *Icarus* **1,** 151–169 (1962).
8. Howard, J. N., Burch, D. E. & Williams, D. Infrared transmission of synthetic atmospheres. Parts I–V. *J. Opt. Soc. Am.* **46,** 186–190, 237–241, 242–245, 334–338, 452–455 (1956).
9. Gilbert, F. Excitation of the normal modes of the Earth by earthquake sources. *Geophys. J. R. Astron. Soc.* **22,** 223–226 (1970).
10. Osaki, Y. in *Progress of Seismology of the Sun and Stars* (eds Osaki, Y. & Shibahashi, H.) 75–86 (Lecture Notes in Physics Vol. 367, Springer, Berlin, 1989).
11. Wielandt, E. & Streckeisen, G. The leafspring seismometer: design and performance. *Bull. Seismol. Soc. Am.* **72,** 2349–2367 (1982).
12. Kamal & Mansinha, L. A test of the superconducting gravimeter as a long-period seismometer. *Phys. Earth Planet. Inter.* **71,** 52–60 (1992).
13. Smith, S. W. IRIS: A program for the next decade. *Eos* **67,** 213–219 (1986).
14. Dziewonski, A. M. & Woodhouse, J. H. An experiment in the systematic study of global seismicity: centroid-moment tensor solutions for 201 moderate and large earthquakes of 1981. *J. Geophys. Res.* **88,** 3247–3271 (1983).
15. Bullen, K. E. & Bolt, B. A. *An Introduction to the Theory of Seismology* 4th edn (Cambridge Univ. Press, 1985).
16. Beroza, G. & Jordan, T. Searching for slow and silent earthquakes using free oscillations. *J. Geophys. Res.* **95,** 2485–2510 (1990).
17. Turcotte, D. L. & Schubert, G. *Geodynamics Applications of Continuum Physics to Geological Problems* (Wiley, New York, 1982).

Acknowledgements. We thank R. Geller, S. Ida, M. Fujimoto and Y. Fukao for comments on this manuscript.

Correspondence and requests for materials should be addressed to N.K. (e-mail: shibata@geo.titech.ac.jp).

Global and local measures of the intrinsic Josephson coupling in $Tl_2Ba_2CuO_6$ as a test of the interlayer tunnelling model

A. A. Tsvetkov*†, D. van der Marel*, K. A. Moler‡, J. R. Kirtley§, J. L. de Boer*, A. Meetsma*, Z. F. Ren‖, N. Koleshnikov¶, D. Dulic*, A. Damascelli*, M. Grüninger*, J. Schützmann*, J. W. van der Eb*, H. S. Somal* & J. H. Wang‖

* *Materials Science Centre, University of Groningen, 9747 AG Groningen, The Netherlands*
† *P. N. Lebedev Physical Institute, 117924 Moscow, Russia*
‡ *Department of Physics, Princeton University, Princeton, New Jersey 08544, USA*
§ *IBM T. J. Watson Research Center, PO Box 218, Yorktown Heights, New York 10598, USA*
‖ *Department of Chemistry, SUNY at Buffalo, Buffalo, New York 14260-3000, USA*
¶ *Institute of Solid State Physics, Russian Academy of Sciences, Chernogolovka, Russia*

One leading candidate theory of high-temperature superconductivity in the copper oxide systems is the interlayer tunnelling (ILT) mechanism[1]. In this model, superconductivity is created by tunnelling of electron pairs between the copper oxide planes—contrasting with other models in which superconductivity first arises by electron pairing within each plane. The ILT model predicts that the superconducting condensation energy is approximately equal to the gain in kinetic energy of the electron pairs due to tunnelling. Both these energies can be determined independently[2–4], providing a quantitative test of the model. The gain in kinetic energy of the electron pairs is related to the interlayer plasma frequency, ω_J, of electron pair oscillations, which can be measured using infrared spectroscopy. Direct imaging of magnetic flux vortices also provides a test[5], which is performed here on the same samples. In the high-temperature superconductor $Tl_2Ba_2CuO_6$, both the sample-averaging optical probe and the local vortex imaging give a consistent value of $\omega_J \approx 28\,cm^{-1}$ which, when combined with the condensation energy, produces a discrepancy of at least an order of magnitude with deductions based on the ILT model.

In the ILT model, the normal state is different in nature from the traditional Landau Fermi liquid. As a result, coherent transport of single charge carriers between the planes is strongly inhibited in the normal state. In the superconducting phase, tunnelling of pairs is possible, and the superconducting condensation energy (E_{cond}) in the ILT model is the gain in kinetic energy (E_J) due to the tunnelling of those pairs: $E_{cond} = \eta E_J$. The number η is of the order of 1 when ILT is the only active pairing mechanism[3]. With conventional mechanisms, although usually $\eta \ll 1$, there is no prediction for η that is free from materials parameters. A crucial point in this discussion is that both E_{cond} and E_J are experimentally accessible quantities, thus allowing the experimental verification of the ILT hypothesis. E_{cond} can be measured from the specific heat[6]; E_J can be determined by measuring the interlayer (Josephson) plasma frequency[7].

For this work, we used two kinds of samples: single crystals and epitaxial thin films of $Tl_2Ba_2CuO_6$. The crystals have a superconducting transition temperature (T_c) of 82 K and transition width (10%–90%) of 13 K, as determined by bulk susceptibility measurements using a superconducting quantum interference device (SQUID). Using 4-circle X-ray diffraction, we verified that the material belongs to the tetragonal *I*4/*mmm* space group, with (for the crystals) lattice parameters $a = b = 3.867$ Å, and $c = 23.223$ Å. The films have $T_c = 80$ K as determined by d.c. resistivity, and $c = 23.14$ Å. Both types of samples have relatively large physical dimensions perpendicular to the *c*-axis, corresponding to the conducting copper oxide planes (50 mm^2 for the thin films, and 1 mm^2 for the crystals). They have small dimensions along the *c*-axis (~1 μm for the thin films, and ~50 μm for the crystals).

To determine the plasma resonance, we measure the reflection coefficient of infrared radiation incident on the *a*–*b*-plane at a large angle (80°) with the surface normal[8]. A sketch of our experiments is shown in Fig. 1. In the case of the single crystals, the intensity of the reflected light drops below our detection limit if the wavelength exceeds 0.2 mm (that is, for $\omega/2\pi c < 50\,cm^{-1}$, where ω is an angular frequency and *c* is the speed of light) due to diffraction. Using thin films we were able to extend this range to 20 cm^{-1}. The electric field vector of the radiation is chosen to be parallel to the plane of incidence, resulting in a large component perpendicular to the CuO_2 planes. This geometry allows absorption of the light by lattice vibrations and plasma-oscillations polarized perpendicular to the planes.

In Fig. 2a we show the single-crystal and thin-film reflectivity for $\omega/2\pi c$ above and below 150 cm^{-1}, respectively. All prominent absorption lines for frequencies above 50 cm^{-1} correspond to infrared-active lattice vibrations, which show no strong temperature dependence. In the 4 K spectrum we observe a clear absorption

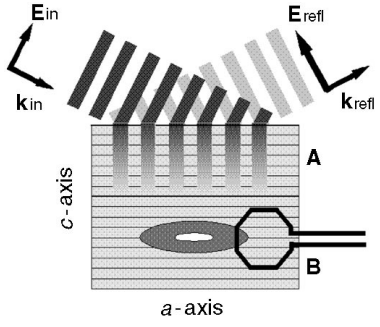

Figure 1 Diagram of the experimental set-up. **A**, Grazing-incidence reflectivity. The p-polarized light incident at a grazing angle sets up a periodic electric field pattern, which is polarized perpendicular to the sample surface, and decays exponentially inside the solid. **B**, Scanning SQUID microscopy. The octagonal pick-up loop detects the magnetic flux perpendicular to the *a*–*c* face.